J Sol-Gel Sci Technol (2015) 74:834–843
DOI 10.1007/s10971-015-3701-9

REVIEW PAPER

Magnetic mesoporous carbon: efficiently reusable adsorbent for ionic liquid [Bmim]Cl from aqueous solution

Jin Hui Tao[1] · Feng Zhang[1] · Qun Feng Yue[1]

Received: 27 October 2014 / Accepted: 1 April 2015 / Published online: 16 April 2015

Abstract Magnetic mesoporous carbon composite (Fe/OMC) was synthesized and as an adsorbent for removal of ionic liquid, 1-butyl-3-methyl imidazolium chloride ([Bmim]Cl), from aqueous solution. X-ray diffraction, transmission electron microscopy analyses and nitrogen adsorption measurements revealed that the synthesized Fe/OMC composite retained ordered mesoporous structure. Meanwhile, nitrogen adsorption measurements indicated that the Fe/OMC possess relatively high surface areas (up to 651 $m^2\ g^{-1}$), pore volumes (up to 0.66 $cm^3\ g^{-1}$) and multimodal mesopore (3.48 and 4.85 nm) and micropore (1.47 and 1.85 nm) distributions of pore sizes. Magnetic measurement revealed the ferromagnetic property of Fe/OMC at room temperature with saturation magnetization value at 26.11 emu g^{-1} which implies that Fe/OMC composite could be separated by ferromagnet. Results of adsorption experiment showed that Fe/OMC composite was high-performance, easily recyclable adsorbent for ionic liquid, [Bmim]Cl, from aqueous solution. In addition, the Langmuir adsorption isotherm was applicable to the removal process; the maximum adsorption capacity value is 238.32 mg g^{-1}. After eight recycle runs, the adsorption capacity was almost at the same value (238.32 mg g^{-1} for the first sorption and 228.21 mg g^{-1} for the eighth times sorption).

Graphical Abstract An efficient magnetically separable sorbent for wastewater treatments was prepared and can be used to remove the ILs, [Bmim]Cl, from aqueous solution. Adsorption capacity of Fe/OMC adsorbent is good for adsorbing [Bmim]Cl after eight recycle runs. Furthermore, the recovered ionic liquid showed results similar to the fresh one.

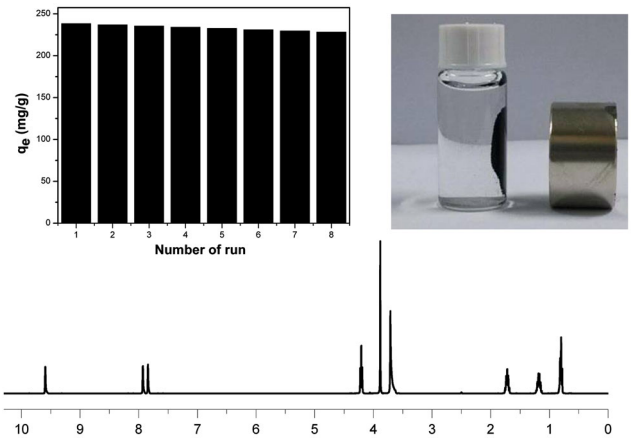

Keywords Magnetic ordered mesoporous carbon · Ionic liquid · Adsorption · Reusable adsorbent

1 Introduction

Ionic liquids (ILs), formerly known as molten salts, constitute one of the hottest areas in chemistry these days. Basically, they have melting points below 100 °C which can be achieved by incorporating a bulky asymmetric cation into the structure together with a weakly coordinating

Electronic supplementary material The online version of this article (doi:10.1007/s10971-015-3701-9) contains supplementary material, which is available to authorized users.

✉ Qun Feng Yue
qfyue@hrbnu.edu.cn

[1] College of Chemistry and Chemical Engineering, Harbin Normal University, Harbin 150025, People's Republic of China

anion. The unique, highly solvable, yet non-coordinating environment of ILs provides an attractive medium for various types of chemical processes. Although ILs can lessen the risk of air pollution due to their insignificant vapor pressure, they do have significant solubility in water. As a result, this is the most likely medium through which ILs will be released into the environment. Since their release to the environment is inevitable, environmental fate and toxicity of ILs have become important topics. Thus, their controlled removal or recovery by oxidation, biodegradation and adsorption from all possible sources, especially water, has been considered, to avoid their long-term adverse consequence to the environment. Some imidazolium ILs have recently been observed to be resistant to photodegradation [1] and biodegradation [2]. But it is important to consider that ILs are still quite expensive and their recycling after regeneration or recovery needs to be regarded. Among available nondestructive technologies, distillation, crystallization, filtration, pervaporation and adsorption onto solid adsorbent are being increasingly studied. Advantage of adsorption is that it can process low concentration of ILs in water solution. According to the recent investigations of many solid compounds, activated carbon (AC) [3–5], ion-exchange resins [6] and montmorillonite [7] have been used as adsorbent for adsorption of ILs from aqueous solution. Owing to its high surface areas and microporous/mesoporous structures, active carbon is widely used for adsorption of organic pollutants from wastewater. Palomar et al. [3] investigated the adsorption of imidazolium-based ionic liquids from aqueous solutions with a commercial AC adsorbent and demonstrated that the size and the hydrophobic nature of both cation and anion of ILs as well as the surface chemistry of AC strongly affect the adsorption capacities. In Palomar' work, AC adsorption quantity for [Bmim]Cl is 0.17 mmol g^{-1} (29.69 mg g^{-1}).

However, AC materials themselves have disadvantageous limitations such as difficulty in collection due to small particle size, high regeneration temperatures and low separation efficiency, usually limiting their application in water treatment. In contrast, mesoporous carbon materials with uniform porosity, high surface area, large pore volume, good thermal stability and chemical inertness have gained increasing attentions in catalysis [8–14], adsorption, host–guest chemistry, environmental technology and biomedical fields [15]. Mitome [16] reported the adsorption behavior of indol from the artificial intestinal juice solution; this result suggests that owing to mesopores and 3D-interconnected pore structures, the amounts of indole adsorbed on mesoporous carbon is significantly higher than the adsorption capacity on AC. Many other reports [17–26] also reported mesoporous carbon as adsorbent for removing contaminants, such as organic dye, antibiotics, phenol and heavy metal ions from a body of water.

As a solid adsorbent in aqueous solution, both AC and mesoporous carbon are difficult to be separated from the liquid phase because of their small particle sizes. An efficient way to solve the problem is to induce magnetic nanomaterials into carbon materials. Due to their unique properties, the magnetic mesoporous carbon materials attract great interests in many fields such as magnetically separable adsorbents, hydrogenation catalyst support and supercapacitors. Nevertheless, the report on using mesoporous carbon and magnetic mesoporous carbon as adsorbents of ionic liquids is not much at present.

In our report, magnetic mesoporous carbon was prepared by a reliable method and used as adsorbent to remove the IL release from aqueous solution. Several methods were used in the preparation of mesoporous carbon materials, such as hard template methods, soft template methods and direct carbonization methods. SBA15 is often used as the template to prepare mesoporous carbon. SBA15 offered a considerable benefit from the ordered pore and hexagonal structure in achieving carbon host. So with that being said, hard template method, mesoporous silica SBA15 as a template, is not only a reproducible method to prepare mesoporous carbon, but also can control the pore size, pore volume and surface area of mesoporous carbon host. Accordingly, SBA15 as the template was chosen to prepare mesoporous carbon host in our paper. 1-Butyl-3-methyl imidazolium chloride ([Bmin]Cl) was chosen as a model ILs, because it is the main ionic liquid used as a starting material in the production of other ionic liquids and also since it is water-soluble and stable with changes in pH and has many uses in processing renewable resources [27].

2 Experimental

2.1 Materials

2.1.1 Preparation of mesoporous carbon

The synthesis of ordered mesoporous carbon was performed using SBA-15 silica as the template and sucrose as carbon source. In a typical reaction process, 1 g SBA-15 and 0.14 g H_2SO_4 were added into 5 mL 0.73 M sucrose solution in a Pyrex beaker. After stirring adequately, the resultant solution was dried at 100 °C for 6 h and then heated to 160 °C 6 h for pre-carbonation. After the solution was naturally cooled down to room temperature, the as-obtained powder was dissolved in 0.8 g of sucrose, 5 g H_2O solution, and subsequently, 0.09 g H_2SO_4 was introduced with stirring; the heat treatment process is same as the above case. Finally, the obtained product was annealed at 900 °C for 6 h under N_2 protection at a ramping rate of

2 °C min^{-1}; subsequently, the SiO_2 template was removed by 10 % HF, and the obtained product was washed with deionized water and dried at 60 °C for a night to obtain the ordered mesoporous carbon, which be signed OMC in this paper.

2.1.2 Preparation of magnetic mesoporous carbon

The magnetic mesoporous carbon materials were synthesized as follows: 0.4 g OMC and 1.4 g $FeCl_3{\cdot}6H_2O$ were dispersed in 75 mL ethylene glycol, by ultrasonication for 2 h. After that, 3.6 g CH_3COONa was added into the solution with ultrasonication for another 2 h, and the obtained solution was then transferred into a stainless autoclave at 200 °C for 16 h. The products were collected with magnet, washed with deionized water for five times and then dried in oven at 50 °C for 8 h, and the magnetic OMC was obtained, which be signed Fe/OMC.

2.1.3 Synthesis of ionic liquid

The ionic liquid, 1-methyl-3-butyl imidazolium chloride ([Bmim]Cl), was synthesized according to the previous literatures [28]. [Bmim]Cl was synthesized by refluxing the 1-methylimidazole with a large excess of the chlorobutane for 24 h. The excess chlorobutane was removed by evaporation, and crude product was recrystallized from acetonitrile/ethyl acetate. The resulting white precipitate was isolated by filtration and then dried in vacuo for 24 h. [Bmim]Cl was characterized by ^{1}H-NMR spectra, and all the peaks were assigned: δ (ppm) 9.16 (*s*, N–CH–N), 7.77 (*s*, CH_3–N–CH–CH), 7.70 (*s*, CH_3–N–CH–CH), 4.18 (*t*, N–CH_2), 3.86 (*s*, N–CH_3), 1.75 (*m*, N–CH_2–CH_2), 1.25 (*m*, CH_2–CH_3) and 0.89 (*t*, CH_2–CH_3).

2.2 Characterization and measurements

X-ray diffraction (XRD) data were collected on a Riguku XDS 2000 diffractometer with Cu Ka, using radiate on at 50 kV and 20 mA. Scanning electron microscopy (SEM) measurements were performed using Hitachi S-480 operating at an accelerating voltage of 15 kV. Transmission electron microscopy (TEM) images were recorded on FeiTecnia G2-STWIN. Thermal gravimetric (TG) experiments were conducted by a Pyris-Diamond TG analyzer in a temperature range of 30–800 °C under an air atmosphere with a heating rate of 10 °C min^{-1}. The nitrogen adsorption–desorption, surface areas and median pore diameters were measured using a Quantachrome NOVA 2000e analyzer. Before being measured at 77 K, the samples were degassed at 423 K for 12 h. Specific surface areas and pore size distributions were calculated using the Brunauer–Emmett–Teller (BET), and density functional theory (DFT) and Barrett–Joyner–Halenda (BJH) models from the adsorption branches, respectively. The magnetic measurements were made on a vibrating sample magnetometer (VSM, Lake Shore, Model 7410). Raman spectroscopy was performed using LabRAM HR 800. Adsorbate concentrations were determined by UV–Vis spectra on Lambda 45 spectrophotometer. ^{1}H NMR spectra of [Bmim]Cl was recorded on a BRUKER AVANCE AV400 spectrometer and calibrated with tetramethylsilane (TMS) as the internal standard.

2.3 Adsorption and desorption experiments

A total of 25 mg adsorbent, OMC or Fe/OMC, was brought into contact with [Bmim]Cl solution in 50-mL flasks. We use commercial AC for a comparison study, and the experimental details are the same in each experiment. The mixture was stirred at 298 k until the equilibrium was reached (typically 18 h). After adsorption, spent Fe/OMC was separated by the external magnetic field, while other adsorbent with centrifugal separation. Adsorbate concentrations were determined by UV spectroscopy at 211 nm, which is the approximate maximum of absorption measured for the imidazolium cations. The equilibrium adsorption capacities (Q_e) were determined according to the following formula:

$$Q_e = \frac{(C_i - C_e)V}{m}$$

wherein C_i and C_e are the initial concentration and residual concentration of [Bmim]Cl respectively, V is the volume of the solution and m is the mass of the adsorbent.

Fe/OMC absorbent as model absorption was studied for researching desorption and repeated use of adsorbent. After the sorption experiments, spent Fe/OMC was separated by the external magnetic field, agitation of Fe/OMC dispersed in 20 mL of ethanol and ultrasonication for 50 min, and then dried in an oven at 100 °C for 24 h. The recycling of Fe/OMC adsorbent for the adsorption–desorption of [Bmim]Cl was studied for eight times. The experiment detail is the same as above.

3 Results and discussion

3.1 Structural feature

Figure 1 shows the powder X-ray diffraction patterns (XRD) of OMC and Fe/OMC. The small-angle XRD pattern of the OMC showed a sharp (100) Bragg reflection with additional peaks corresponding to the (110) and (200) reflections (Fig. 1a), and after the loading of the magnetic

particles, a decrease in the intensity of the XRD reflections was noted. This was probably related to a decreased electron contrast between the channel pores and the walls of the mesoporous materials due to the presence of the bulky organic groups or due to a loss of structural order as a result of the grafting conditions. The wide-angle XRD pattern of Fe/OMC showed a broad diffraction peak at 43.342° attributed to peak of amorphous carbon (Fig. 1b). The characteristic diffraction peaks at 18.391°, 30.272°, 35.741°, 43.342°, 53.852°, 57.399°, 63.012°, 71.527° and 74.539° corresponding to (113), (206), (119), (0012), (2212), (1115), (4012), (2018) and (3315) reflections were well indexed to the face-centered cubic-structured magnetite γ-Fe_2O_3 (JCPDS file No. 25–1402). Based on Scherrer's formula, the Fe_2O_3 particle size is about 13 nm.

Figure 2 shows the SEM and TEM images of synthesised OMC and Fe/OMC. Figure 2a showed that the OMC presents a bamboo-like morphology and relatively smooth surface. After loaded with magnetic particles, it is clearly seen that extraordinarily fine particles are homogeneously

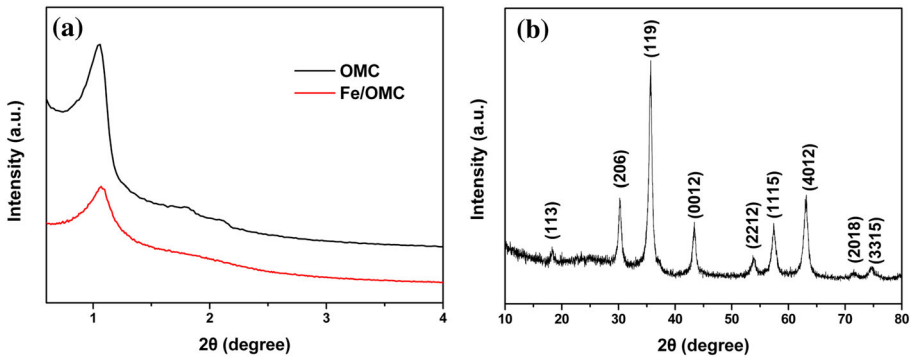

Fig. 1 **a** Small-angle XRD patterns of OMC and Fe/OMC. **b** Wide-angle XRD patterns of Fe/OMC composites

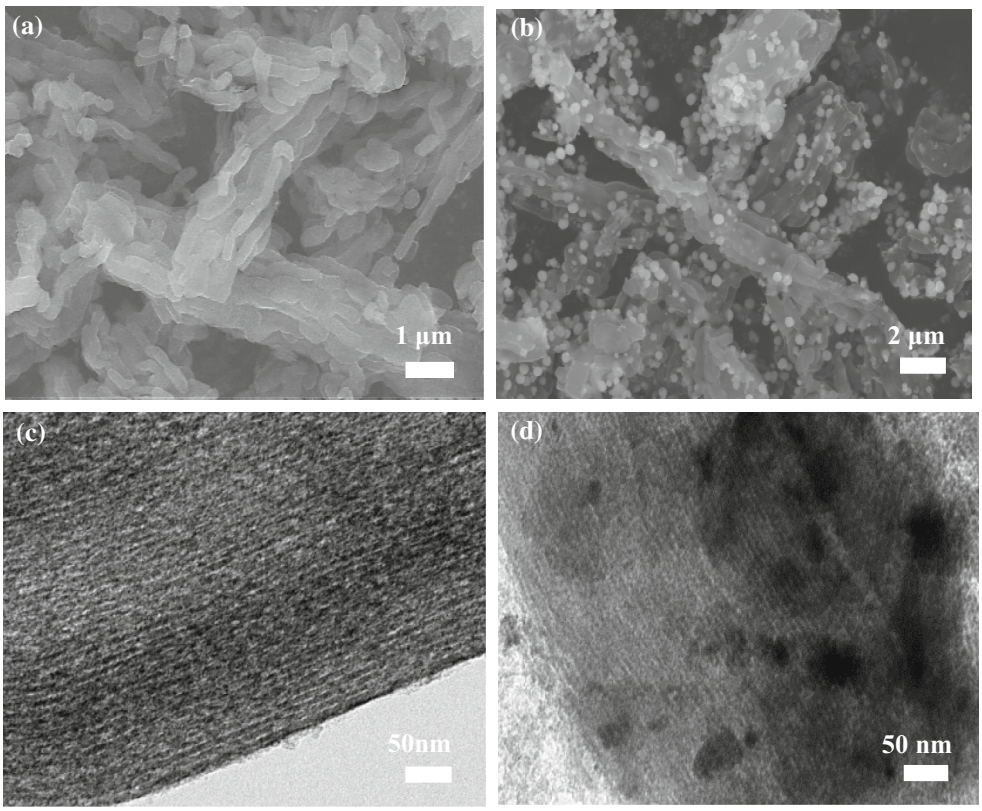

Fig. 2 SEM images of OMC (**a**) and Fe/OMC (**b**). TEM images of OMC (**c**) and Fe/OMC (**d**)

dispersed on the carbon matrix (Fig. 2b). TEM characterizations further present the structural features of the composite, as seen in Fig. 2c, d. It can be seen from Fig. 2c that the OMC exhibits an ordered array of mesoporous channel structure. The carbon arrays are interconnected with each other to form a three-dimensional (3D) network. TEM images of Fe/OMC composites are shown in Fig. 2d. The Fe nanoparticles, which were clearly observed, were embedded in the carbon wall. These images show that most of the Fe_2O_3 is present as submicronic particles. This is probably the main reason why the specific surface area is decreased by 40 % (from the BET results). Compared with carbon arrays in TEM images, the ordering decreased with metal loaded. The TEM results were consistent with the low-angle XRD analysis.

The content of Fe_2O_3 in the composite is estimated by thermogravimetric analysis in a temperature range of 30–800 °C under an air atmosphere with a heating rate of 10 °C min^{-1} (Fig. 3). The small mass loss before 200 °C can be attributed to dehydration. And when the sample is heated to 800 °C, the carbon is oxidized to CO_2. The remaining weight of Fe_2O_3 is 43.93 % (at 630 °C). Accordingly, the content of carbon is about 56.07 wt%.

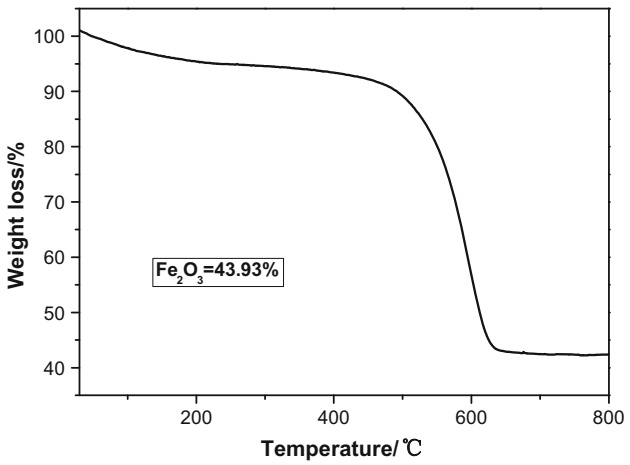

Fig. 3 TG profile of Fe/OMC composite up to 800 °C in air

The pore structures of the OMC and Fe/OMC were further analyzed using nitrogen sorption measurements. All the samples were degassed at 423 K for 12 h on a vacuum line before being measured. Figure 4 shows nitrogen adsorption–desorption isotherms (Fig. 4a) and pore size distributions (Fig. 4b) of OMC and Fe/OMC, respectively. As displayed in Fig. 4a, it can be seen that OMC sample exhibits type IV isotherms with H4-type hysteresis loops at high relative pressure region, suggesting that the mesoporous structure exists at OMC sample. As shown in Fig. 4b, the OMC, carbon host, has a pore size distribution centered at 3.90 nm according to the BJH method. For magnetic mesoporous carbon, Fe/OMC, the isotherm is of type II because of no plateau (Fig. 4a). Apparently, the pore structure of the mesoporous carbon host was destroyed during the precipitation of Fe_2O_3 nanoparticles, possibly due to the etching of the carbon walls during the reaction process. The primary pore diameters of Fe/OMC material are evaluated as 3.48 and 4.85 nm (Fig. 4b) according to the BJH models, and those of it has two maxima at 1.47 and 1.85 nm attributed to micropore of Fe/OMC (Fig. 4b inset) using the NLDFT method, which reveals

Table 1 Comparison of textural properties between OMC and Fe/OMC

Sample	S_{BET} (m^2 g^{-1})	Pore size (nm)	Pore volume (cm^3 g^{-1})
OMC	1010	3.90	1.24
Fe/OMC	651	3.48/4.85[a]	0.66

[a] According to the BJH method

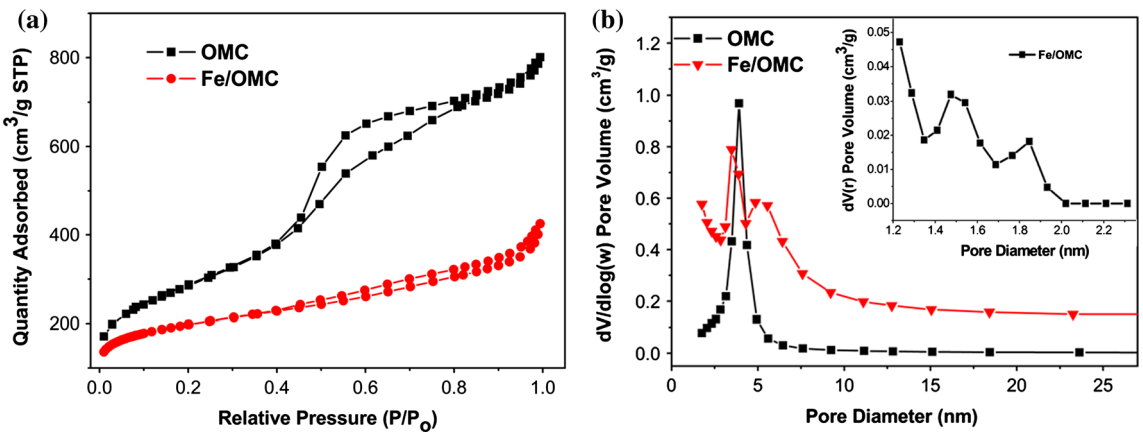

Fig. 4 N_2 adsorption–desorption isotherms (**a**) and pore size distributions (**b**) of OMC and Fe/OMC using Barrett–Joyner–Halenda (BJH) method. *Inset* pore size distributions of Fe/OMC according non-local density functional theory (NLDFT) method

that the micropore and mesopore structures are included in Fe/OMC materials. The BET surface areas of OMC and Fe/OMC are 1010 and 651 $m^2\ g^{-1}$, and the corresponding pore volumes are 1.25 and 0.66 $cm^3\ g^{-1}$, respectively. The specific surface area and the specific pore volume of Fe/OMC are much lower than those of OMC, which confirms the framework collapse during the precipitation of Fe_2O_3 nanoparticles. The textural properties of OMC and Fe/OMC are summarized in Table 1.

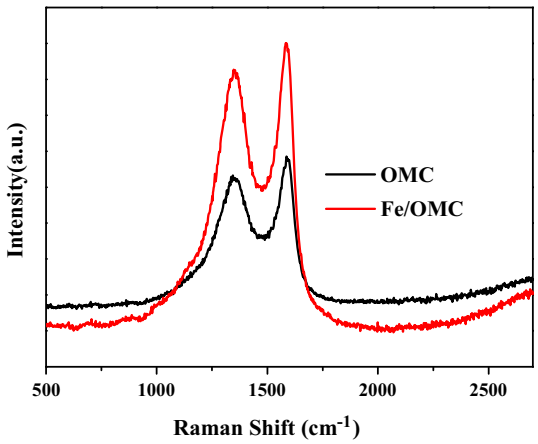

Fig. 5 Raman spectrum of the OMC and Fe/OMC

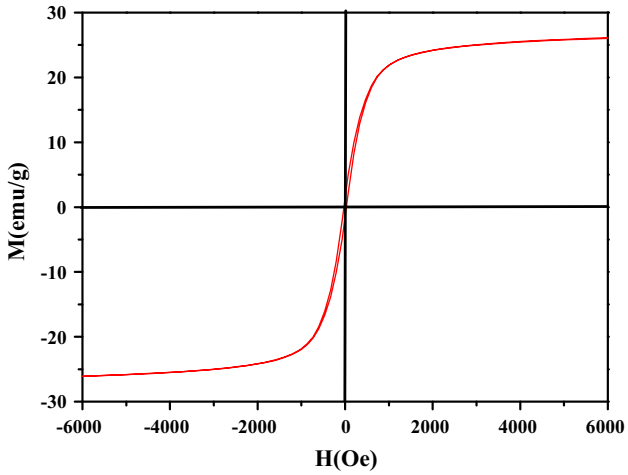

Fig. 6 Magnetization curves of Fe/OMC

Raman spectra of OMC and Fe/OMC were measured and compared. As shown in Fig. 5, both samples exhibited the peaks at 1350 and 1590 cm^{-1}, corresponding to so-called D and G bands. The D band is usually associated with the vibrations of carbon atoms with dangling bonds for the in-plane terminations of disordered graphite. The G band is due to the sp^2-bonded carbon–carbon stretching (E_{2g}) mode in a two-dimensional hexagonal lattice for graphene sheet. The intensity ratio of the D and G bands (ID/IG) has a physical meaning for the crystallinity or amorphicity of carbon materials. This ID/IG value calculated from Fig. 5 is found to be $R_1 = 0.90$, $R_2 = 0.92$, implying crystallinity to some extent. Such values indicate that iron may catalytically graphitize the OMC. The ID/IG of Fe/OMC was slightly larger than that of the OMC sample, which suggested the carbon in Fe/OMC sample was more disordered because of the induced magnetic composition, in agreement with XRD result.

The magnetization curves (Fig. 6) for sample presented almost no hysteresis loop, indicating that the samples exhibited superparamagnetic characteristics desirable for application in separation under an external magnetic field. Superparamagnetism is the responsiveness to an applied magnetic field after removal of the applied magnetic field. The typical ferromagnetic curve of the sample Fe/OMC exhibited a saturation magnetization value at 26.11 e-mu g^{-1} (Fig. 6). It is well known that superparamagnetic nanocomposite can be easily separated by magnet.

Figure 7 is the photograph of Fe/OMC in wastewater and under an external magnet. The powder Fe/OMC could be easily separated from the solution by an external magnet. The property of magnetic attraction is quite useful for the separation of carbon in adsorption processes.

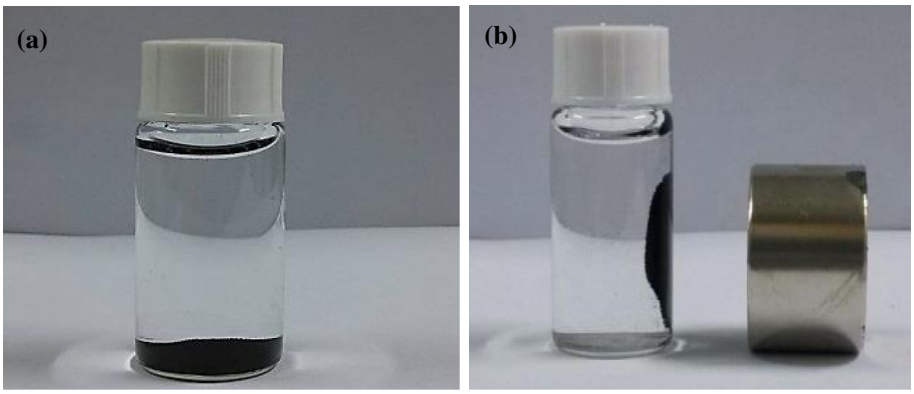

Fig. 7 Photograph of Fe/OMC in wastewater and under an external magnet

3.2 Adsorption of [Bmim]Cl

The relationship between the adsorption capacity and the adsorption time was investigated in Fig. 8. As can be seen from Fig. 8a, after achieving adsorption equilibrium, adsorption amount of Fe/OMC was higher than OMC absorbent. Although the specific surface area of OMC is 1010 $m^2\ g^{-1}$, greater than that specific surface area of Fe/OMC (654 $m^2\ g^{-1}$), based on BET test results, the adsorption amount is smaller than Fe/OMC absorbent.

Coutinho et al. [29] reported theirs researches about adsorption of ionic liquids onto AC by the addition of inorganic salts. In Coutinho's work, the salting-out ability of an inorganic salt, Na_2SO_4, a strong salting-out-inducing salt that does not change the medium pH when dissolved in aqueous medium, was used to improve the adsorption of different ILs (hydrophobic and hydrophilic) onto AC. It was already shown that Na_2SO_4 can promote the phase separation when combined with hydrophilic ILs in aqueous solutions and that it can decrease the solubility of highly hydrophobic and fluorinated ILs in water. From another view, hydrophily of mesoporous carbon host is increased by doping Fe_2O_3 particles. We speculate that increase in hydrophilic mesoporous carbon host maybe is one of the main reasons for higher adsorption amount of Fe/OMC than OMC adsorbent. However, detailed relationship between the hydrophily of mesoporous carbon host and the amount of adsorption of ILs in aqueous solution needs further study in our following works.

A commercial AC with high surface area (781 $m^2\ g^{-1}$, Fig. S1) was used for adsorption of [Bmim]Cl when compare with prepared Fe/OMC adsorbent. The maximum adsorption amount of AC is only about 107.04 mg g^{-1} (Fig. S2). Obviously, AC shows lower adsorption capacity than Fe/OMC samples. For AC, the presence of lots of micropores is not conducive to the adsorption of ionic liquids [3]. So the results demonstrate that the Fe/OMC has the great potential in ILs adsorption.

The adsorption isotherm experimental data were collected at different concentrations of [Bmim]Cl as shown in Fig. 8b. It can be seen from Fig. 8b that the adsorption amount increases with the increase in IL concentration until the adsorption reaches saturation (297.9 mg L^{-1}). The materials show nearly complete adsorption with the initial concentration below 200 mg L^{-1} as shown in Fig. 8b. To

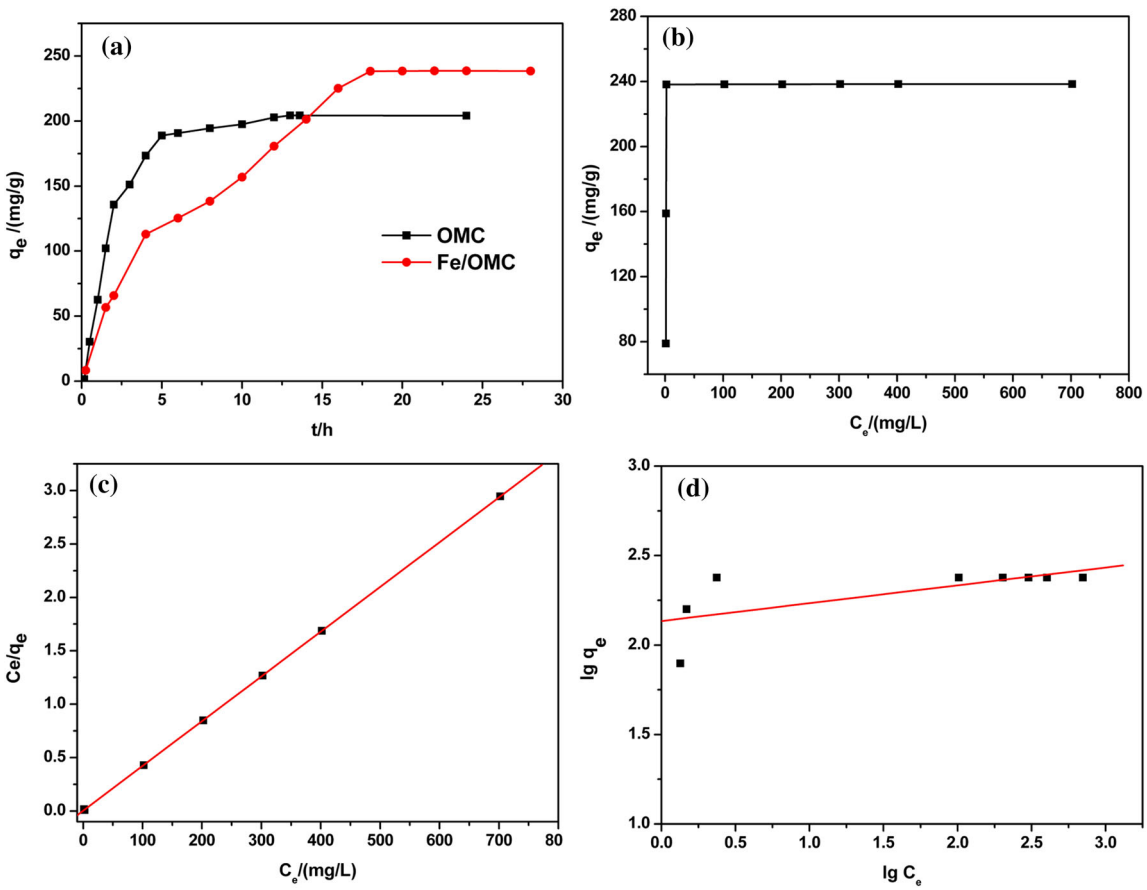

Fig. 8 **a** Relationship between the adsorption capacity and the adsorption time. **b** Adsorption capacities for [Bmim]Cl on Fe/OMC. Langmuir (**c**) and Freundlich (**d**) fits (*curves*) for the adsorption of [Bmim]Cl

examine the efficiency of the prepared Fe/OMC adsorbent, adsorption isotherms were fitted to Langmuir and Freundlich models given by Eqs. (1) and (2), respectively.

$$\frac{C_e}{q_e} = \frac{1}{bq_m} + \frac{C_e}{q_m} \quad (1)$$

$$\lg q_e = \lg k_f + \frac{1}{n}\lg C_e \quad (2)$$

where C_e is the equilibrium concentration (mg L^{-1}) of ionic liquid in solution, q_e is the equilibrium adsorption amount (mmol g^{-1}), q_m is the maximum adsorption capacity (mg g^{-1}), b is the adsorption equilibrium constant (L $mmol^{-1}$), K_f is a constant representing adsorption capacity (L $mmol^{-1}$) and n is an indication of linearity. Figure 8c, d is the linear Langmuir and Freundlich models of the isotherms, and the parameters of Langmuir and Freundlich are given in Table 2. From Table 2, the Langmuir model, typical monolayer adsorption, could provide better representation of the adsorption isotherms of [Bmim]Cl than the Freundlich model. That is to say, in this paper, the adsorption behaviors belong to the monolayer adsorption. Maximum adsorption capacity q_m, was calculated for adsorbents with the Langmuir model so that their adsorption capacity could be compared (Table 2). Comparing theoretical maximum adsorption capacities (Table 2, 238.66 mg g^{-1}) with the experimental maximum adsorption capacities (Fig. 8b, 238.32 mg g^{-1}), the experimental value is near the theoretical value. This confirms that the adsorption of [Bmin]Cl on Fe/OMC adsorbent fits the typical Langmuir adsorption model well in aqueous solution.

Table 2 Fitting parameters of the Langmuir and Freundlich equations for [Bmin]Cl sorption onto the prepared Fe/OMC adsorbent

Langmuir model			Freundlich model		
Q_m	b	R	K_F	n	R
238.66	1.24	0.99	136.19	10.03	0.68

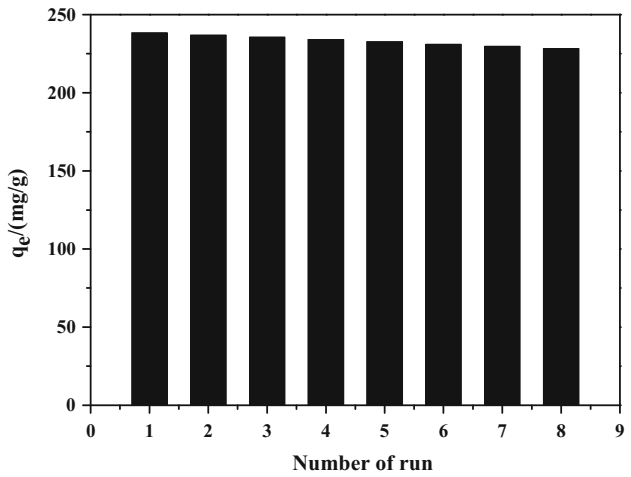

Fig. 9 Adsorption cycles of the prepared Fe/OMC for [Bmim]Cl

3.3 Adsorbent regeneration and IL recovery

Regeneration of an exhausted adsorbent for reuse is a determining factor regarding its potential application at industrial scale. If adsorption is to be applied for ILs, the recovery of this type of adsorbent becomes a critical point due to their high value and toxicity which would give the characteristic of toxic waste to the exhausted adsorbent. In this section, both adsorption performance of the regenerative Fe/OMC adsorbents and the later recovery of an ILs of reference, [Bmim]Cl, have been checked. Figure 9 shows the results of adsorption capacity of [Bmin]Cl on regeneration adsorbent in aqueous solution. From Fig. 9, after eight sorption–desorption cycles, the adsorption capacity is almost the same value (238.32 mg g^{-1} for the first sorption and 228.21 mg g^{-1} for the eighth sorption).

To check for recovery of ionic liquid [Bmim]Cl, we used UV–vis spectra at room temperature and tested the ionic liquid concentration before adsorption, after adsorption and desorption, respectively. Hence, concentration was evaluated base on Lambert–Beer's law:

$$A = k \cdot b \cdot C$$

where A is absorbency and C is the concentration of the measured solution. The initial concentration of [Bmin]Cl before adsorption, C_0 is 1000 mg L^{-1}, the equilibrium concentration of [Bmin]Cl after adsorption C_e and the concentration of [Bmin]Cl after desorption C_d are listed in Table 3, and C_e and C_d is the relationship between $C_d + C_e = C_0$ theoretically. The sorption–desorption process was carried out five times in parallel, and average value of $C_d + C_e = C_0$ is 993.94 mg L^{-1}. Obviously,

Table 3 Concentration of [Bmin]Cl before and after adsorbed

Times of experiments	C_e	C_d	$C_d + C_e$	Average value of ($C_d + C_e$)
1	702.10	297.90	1000.00	993.94
2	702.22	288.9	991.12	
3	702.26	288.5	990.76	
4	701.94	291.84	993.78	
5	701.96	292.06	994.02	

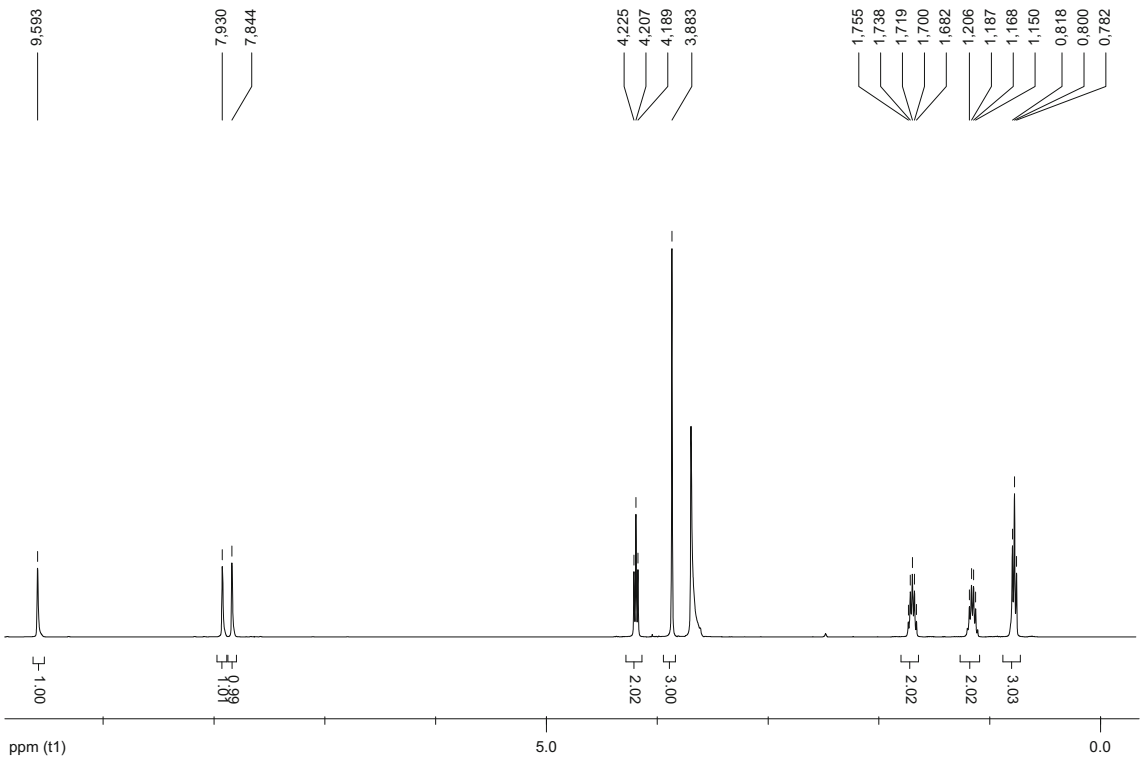

Fig. 10 ^{1}H NMR spectrum of [Bmim]Cl after desorption

these three values with the following relations: $C_d + C_e = C_0$ suggest that after a sorption–desorption cycles, recovery of ionic liquid [Bmim]Cl is good.

Moreover, we characterized the recovered [Bmim]Cl by NMR (Fig. 10). It was found that the recovered ionic liquid showed results similar to the fresh one. Consequently, renewable and recyclable Fe/OMC adsorbents exhibited a great promising application in IL-contaminated water attributed to its high adsorption capacity and facile separation.

4 Conclusion

In conclusion, we first report a reliable and simple method to synthesize magnetic mesoporous carbon (Fe/OMC) used as adsorbent to remove the ILs, [Bmim]Cl, from aqueous solution. The structure test shows that Fe/OMC has ordered mesoporous structure and high surface area (651 $m^2\ g^{-1}$). Furthermore, the Fe/OMC composite with a saturation magnetization of 26.11 emu g^{-1} implies that Fe/OMC composite could be separated by magnet from solution. Although the specific surface area of Fe/OMC is decreased by 40 %, adsorption amount of Fe/OMC (238.32 mg g^{-1}) on ILs is the relatively highest, compared with those of OMC (204.24 mg g^{-1}) and AC (107.04 mg g^{-1}). It is worth mentioning that adsorption capacity of Fe/OMC adsorbent is good for adsorbing [Bmim]Cl after eight recycle runs. The above results demonstrate that the as-prepared magnetic mesoporous carbon is an efficient magnetically separable sorbent for wastewater treatments.

Acknowledgments This work was financial supported by Pre-research fund for the Technology Development of Harbin Normal University (To support in 2015) and Doctor Funding of Harbin Normal University (No. XKB201310).

References

1. Stepnowski P, Zaleska A (2005) Comparison of different advanced oxidation processes for the degradation of room temperature ionic liquids. J Photochem Photobiol A 170:45–50
2. Gathergood N, Scammells PJ (2002) Design and preparation of room-temperature ionic liquids containing biodegradable side chains. Aust J Chem 55:557–560
3. Palomar J, Lemus J, Gilarranz MA, Rodriguez JJ (2009) Adsorption of ionic liquids from aqueous effluents by activated carbon. Carbon 47:1846–1856
4. Lemus J, Palomar J, Gilarranz MA, Rodriguez JJ (2013) On the kinetics of ionic liquid adsorption onto activated carbons from aqueous solution. Ind Eng Chem Res 52:2969–2976
5. Lemus J, Palomar J, Heras F, Gilarranz MA, Rodriguez JJ (2012) Developing criteria for the recovery of ionic liquids from aqueous phase by adsorption with activated carbon. Sep Purif Technol 97:11–19

6. Choi SB, Won SW, Yun YS (2013) Use of ion-exchange resins for the adsorption of the cationic part of ionic liquid 1-ethyl-3-methylimid azolium. Chem Eng J 214:78–82
7. Reinert L, Batouche K, Lévêque JM, Muller F, Bény JM, Kebabi B, Duclaux L (2012) Adsorption of imidazolium and pyridinium ionic liquids onto montmorillonite: characterisation and thermodynamic calculations. Chem Eng J 209:13–19
8. Yuan DS, Yuan XL, Zou WJ, Zeng FL, Huang XJ, Zhou SL (2012) Synthesis of graphitic mesoporous carbon from sucrose as a catalyst support for ethanol electro-oxidation. J Mater Chem 22:17820–17826
9. Liu L, Deng QF, Agula B, Ren TZ, Liu YP, Zhaorigetu B, Yuan ZY (2012) Synthesis of ordered mesoporous carbon materials and their catalytic performance in dehydrogenation of propane to propylene. Catal Today 186:35–41
10. Horváth E, Puskás R, Rémiás R, Mohl M, Kukovecz A, Kónya Z, Kiricsi I (2009) A novel catalyst type containing noble metal nanoparticles supported on mesoporous carbon: synthesis, characterization and catalytic properties. Top Catal 52:1242–1250
11. Shanahan PV, Xu LB, Liang CD, Waje M, Dai S, Yan (2008) Graphitic mesoporous carbon as a durable fuel cell catalyst support. J Power Sources 185:423–427
12. Mahata N, Goncalves F, Pereira MFR, Figueiredo JL (2008) Selective hydrogenation of cinnamaldehyde to cinnamyl alcohol over mesoporous carbon supported Fe and Zn promoted Pt catalyst. Appl Catal A 339:159–168
13. Selvam P, Kuppan B (2012) Synthesis, characterization and electrocatalytic properties of nano-platinum-supported mesoporous carbon molecular sieves s, Pt/NCCR-41. Catal Today 198:85–91
14. Long DH, Chen QJ, Qiao WM, Zhan L, Liang XY, Ling LC (2009) Three-dimensional mesoporous carbon aerogels: ideal catalyst supports for enhanced H_2S oxidation. Chem Commun 26:3898–3900
15. Wang TY, Zou MJ, Jiang HT, Ji ZS, Gao P, Cheng G (2011) Synthesis of a novel kind of carbon nanoparticle with large mesopores and macropores and its application as an oral vaccine adjuvant. Eur J Pharm Sci 44:653–659
16. Mitome T, Uchida Y, Egashira Y, Hayashi K, Nishiura A, Nishiyama N (2013) Adsorption of indole on KOH-activated mesoporous carbon. Coll Surf A Physicochem Eng Asp 424:89–95
17. Dong Y, Lin HM, Qu FY (2012) Synthesis of ferromagnetic ordered mesoporous carbons for bulky dye molecules adsorption. Chem Eng J 193–194:169–177
18. Wang TB, Liang L, Wang RW, Jiang YQ, Lin KF, Sun JM (2012) Magnetic mesoporous carbon for efficient removal of organic pollutants. Adsorption 18:439–444
19. Li JT, Li BL, Wang HC, Bian XB, Wang XM (2011) A wormhole-structured mesoporous carbon with superior adsorption for dyes. Carbon 49:1912–1918
20. He C, Hu XJ (2012) Functionalized ordered mesoporous carbon for the adsorption of reactive dyes. Adsorption 18:337–348
21. Teng MM, Qiao JL, Li FT, Bera PK (2012) Electrospun mesoporous carbon nanofibers produced fromphenolic resin and their use in the adsorption of large dye molecules. Carbon 50:2877–2886
22. Shi S, Fan YW, Huang YM (2013) Facile low temperature hydrothermal synthesis of magnetic mesoporous carbon nanocomposite for adsorption removal of ciprofloxacin antibiotics. Ind Eng Chem Res 52:2604–2612
23. Sun ZH, Wang LF, Liu PP, Wang SC, Sun B, Jiang DZ, Xiao FS (2006) Magnetically motive porous sphere composite and its excellent properties for the removal of pollutants in water by adsorption and desorption cycles. Adv Mater 18:1968–1971
24. Lee HI, Jung YJ, Kim S, Yoon JA, Kim JH, Hwang JS, Yun MH, Yeon JW, Hong CS, Kim JM (2009) Preparation and application of chelating polymer–mesoporous carbon composite for copper-ion adsorption. Carbon 47:1043–1049
25. Ni YH, Jin L, Zhang L, Hong JM (2010) Honeycomb-like Ni@C composite nanostructures: synthesis, properties and applications in the detection of glucose and the removal of heavy-metal ions. J Mater Chem 20:6430–6436
26. Zhuang X, Wan Y, Feng CM, Shen Y, Zhao DY (2009) Highly efficient adsorption of bulky dye molecules in wastewater on ordered mesoporous carbons. Chem Mater 21:706–716
27. Vijayaraghavan K, Pham TPT, Cho CW, Won SW, Choi SB, Juan M, Kim S, Kim YR, Chung BW, Yun YS (2009) An assessment on the interaction of a hydrophilic ionic liquid with different sorbents. Ind Eng Chem Res 48:7283–7288
28. Bonhôte P, Dias AP, Papageorgiou N, Kalyanasundaram K, Grätzel M (1996) Hydrophobic, highly conductive ambient-temperature molten salts. Inorg Chem 35:1168–1178
29. Neves CMSS, Lemus J, Freire MG, Palomar J, Coutinho JAP (2014) Enhancing the adsorption of ionic liquids onto activated carbon by the addition of inorganic salts. Chem Eng J 252: 305–310